

Traceability of S-Parameter Measurements Up to 167 GHz Using 0.8 mm Coaxial Standards

Andreas Tobias Schramm^{ID}, *Member, IEEE*, Frauke Kathinka Helene Gellersen^{ID}, Florian Rausche, and Karsten Kuhlmann^{ID}

Abstract—To establish traceable S-parameter measurements in the 0.8 mm coaxial connector system, dimensional measurements are performed on a set of seven offset short standards. Reflection coefficients for each standard are calculated numerically and analytically based on these dimensions. S-parameter measurements are conducted for one-port devices up to 167 GHz, and an optimization-based calibration is applied, treating material properties as free parameters. Selected measurement results are presented, and associated uncertainty budgets are discussed.

Index Terms—Coaxial, least-squares calibration, offset short, S-parameter, traceability, vector network analysis.

I. INTRODUCTION

THE ongoing development toward the sixth generation (6G) of mobile communication systems necessitates advancements in high-frequency metrology, particularly for high-frequency base quantities such as RF power [1] and S-parameters [2]. Achieving traceability of these quantities to the *Système International d'Unités* (SI, International System of Units) is essential for maintaining comparability between laboratories and manufacturers in a globalized world.

Established coaxial precision connectors (PCs) like PC 1.35 and 1.0 mm are standardized up to 90 and 110 GHz, respectively [3]. Traceability for these connectors is demonstrated in [4] and [5]. In [2], the possibility to achieve traceable reflection coefficient measurements (s_{11}) up to 165 GHz for the 0.8 mm PC was demonstrated. While it laid out the foundation for PC 0.8 mm also standardized [3] since 2022, the connection repeatability was somewhat limited by the temperature fluctuations during the measurement. The maximum achievable frequency was 165 GHz and no additional two-port devices under test (DUTs) were measured.

Several improvements have been realized since, which are thoroughly discussed in this work. These include excellent connection repeatability, an increase of the upper calibration frequency limit from 165 to 167 GHz, new commercially available calibration standards specified and measured up to 167 GHz, and the extension of S-parameter measurement capabilities to transmission coefficients. The design and calculation

Received 4 July 2025; revised 29 August 2025; accepted 18 September 2025. Date of publication 3 October 2025; date of current version 11 December 2025. This work is part of the project 23IND03 *RF46G* focussing on advancing key quantities for 6G. The project 23IND03 *RF46G* has received funding from the European Partnership on Metrology, co-financed from the European Union's Horizon Europe Research and Innovation Programme and by the Participating States. (Corresponding author: Andreas Tobias Schramm.)

The authors are with the Physikalisch-Technische Bundesanstalt (PTB), 38116 Brunswick, Germany (e-mail: andreas.schramm@ptb.de).

Digital Object Identifier 10.1109/TMTT.2025.3613009



Fig. 1. Primary offset shorts (C2–C8, standing) with offset lengths between 1.153 and 10.000 mm. A flush short (C1, lying) is used as verification.

process of the primary calibration standards is extended upon in Section II; dimensional measurement techniques and modeling of the effective conductivity are presented. Section III showcases the measurement setup and resulting improvements in connection repeatability. An initial temperature study regarding short-term phase drift is conducted. The optimization calibration process for the overdetermined least-squares calibrations defined in [6] is presented. Calibration results, including uncertainty budgets, are discussed in Section IV for flush short, broadband open, and broadband match DUTs and are extended by two-port measurements exemplified by a beatty line, where applicable, comparisons to [2] are made.

All measurement uncertainty calculations described in this work are performed using the UncLib [7] by METAS in conjunction with MATLAB [8]. CST Microwave Studio [9] is used to simulate connector effects. Procedures given in [10] and VNA Tools II [11] by METAS are used to evaluate uncertainties of the vector network analyzer (VNA) setups.

II. PRIMARY STANDARD DEFINITION

Only plug standards are used during the primary calibration for the 0.8 mm PC. Seven offset shorts (C2–C8) shown in Fig. 1 are calculated analytically. A flush short (C1) is measured additionally for verification. The lengths and number of standards are optimized to achieve a well-defined system of equations during calibration as well as a large calibration bandwidth. In total, seven offset shorts with nominal and measured lengths summarized in Table I are employed to achieve a calibration bandwidth ranging from 10 GHz to possibly 169.7 GHz, which is the theoretical cutoff frequency of the TE_{11} mode for an ideal 0.8 mm coaxial line with a characteristic impedance of 50 Ω .

Fig. 2 shows the normalized determinant of the Fisher information matrix, which, for $n = 7$, is well above 0.5 for

TABLE I
NOMINAL AND MEASURED OFFSET LINE LENGTHS FOR PC 0.8 MM

offset short	C2	C3	C4	C5	C6	C7	C8
nominal / mm	1.153	3.036	3.890	4.554	5.179	7.634	10.000
measured / mm	1.159	3.041	3.893	4.559	5.180	7.638	10.001

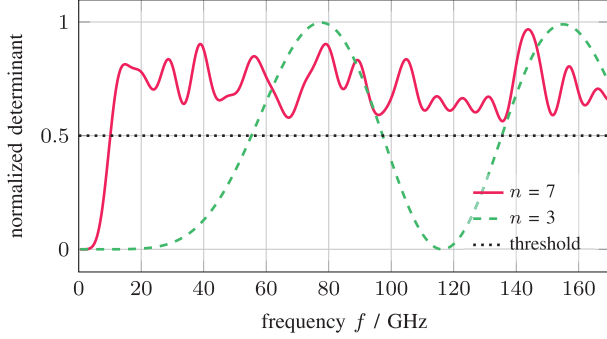


Fig. 2. Determinant of the Fisher information matrix of line length optimization according to [13] for $n = 7$ and $n = 3$ offset shorts. The frequency range for valid calibration is defined by a threshold of 0.5. A subset of three offset shorts with lengths 3.890, 4.554, and 5.179 mm only allows for calibration within a much smaller frequency range.

the optimized frequency range using [12], [13]. The minimum number of standards required to calculate the error terms *directivity* e_{00} , *reflection tracking* $e_{10}e_{01}$, and *source match* e_{11} is 3 [14, p. 132]. However, a restriction of triple offset short calibration is the limited bandwidth, because of the phase relation between the offset shorts. This case is additionally shown in Fig. 2, where a subset ($n = 3$) of the seven optimized offset lengths is used: 3.890, 4.554, and 5.179 mm. Three standards usually offer an uninterrupted relative bandwidth of approximately 1:1.75. Only by adding more offset shorts can one increase the calibration bandwidth.

A. Dimensional Measurements

The characteristic impedance of a coaxial line is dependent on the outer conductor inner diameter (OCID) and the inner conductor outer diameter (ICOD) [15, p. 56]. To establish traceability to the SI, these dimensions are measured along the length of the coaxial standard using traceable dimensional standards calibrated at PTB. These standards are used to calibrate the measurement setups. At each position with a spatial resolution of 10 μm along the length of the coaxial line, the OCID and ICOD of the DUT are measured at several angular positions. The standard deviation is a Type A uncertainty contribution to the measurement result.

The ICOD is measured optically using an optical LED micrometer device. The systematic Type B uncertainty of the measurement setup is characterized to be 0.2 μm . It includes long-term as well as short-term drift effects. Traceability to the SI unit of length is ensured using six plug gauge standards: three close to the nominal ICOD of 0.348 mm and three additional ones close to the nominal pin diameter of 0.200 mm. Expanded uncertainties ($k = 2$) of 1.3 μm are achieved.

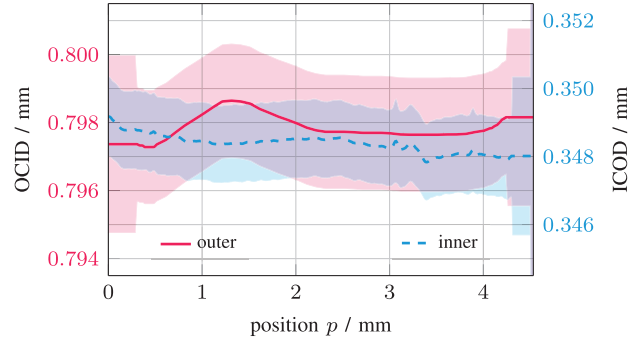


Fig. 3. Dimensional measurement results for OCID and ICOD of a primary offset standard used during primary calibration. The interface of the plug standard is located on the left side ($p = 0$ mm); the short plane is on the opposite side ($p \approx 4.554$ mm). Shaded areas represent expanded uncertainty regions ($k = 2$) according to [16].

The OCID is measured in a contactless manner using air gauging. The systematic Type B uncertainty of the measurement setup is characterized to be 0.4 μm . Traceability is established using three gauge ring standards close to the nominal OCID of 0.800 mm. However, due to the size of the nozzles on both sides of the air probe, some averaging is observed. Several angular positions are measured, but no angular dependencies, e.g., elliptic structures, could be observed due to the geometry of the air probe. Expanded uncertainties ($k = 2$) of 1.8 μm are achieved.

The length of the outer conductor is measured using a tactile system, with gauge blocks serving as traceable calibration standards. Each DUT is measured several times. Table I summarizes the nominal lengths and the measured lengths of the manufactured outer conductors. The maximum difference is 6 μm with an achieved expanded uncertainty ($k = 2$) of 5 μm . The pin depth is measured using a laser scanning microscope, with an expanded uncertainty ($k = 2$) of 2 μm . All offset shorts show a pin depth of at least 10 μm and exceed the minimal pin depth observed in [2].

The measurement results, including expanded uncertainties ($k = 2$) of OCID and ICOD of the standard with a nominal length of 4.554 mm, are shown in Fig. 3. Uncertainties from statistical analysis, systematic influences, as well as calibration standards used are propagated in accordance with [16]. The outer conductor is roughly 2 μm smaller than the nominal value defined in [3]. However, accurate knowledge of the actual geometry is the decisive factor and takes precedence over strict adherence to the nominal geometry. At both ends of the outer conductor, extrapolation is performed to take into account the limitations of the measurement setup described above. Expanded uncertainties of around 1.8 μm for the line segment and 2.7 μm in the extrapolated region are achieved. The inner conductor exhibits a more uniform diameter profile. Especially in the vicinity of the short plane ($p \approx 4.554$ mm, right side), nominal values as defined in [3] are measured. At the short plane, extrapolation is needed because the LED- μm setup exhibits artifacts at steep discontinuities. Expanded uncertainties of around 1.3 μm for the line segment and 2.5 μm in the extrapolated region are achieved.

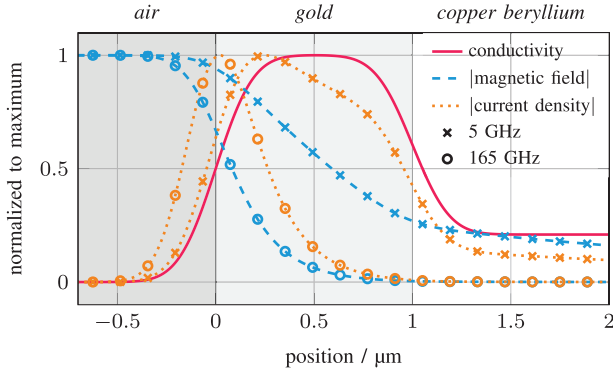


Fig. 4. Exemplary modeling of the effective conductivity of a two-layer system consisting of copper–beryllium ($\sigma_{dc} = 9$ MS/m) coated with gold ($\sigma_{dc} = 43$ MS/m and $h = 1$ μ m). The roughness of both materials is assumed to be 150 nm. In addition, the magnitudes of the magnetic field $|B|$ and the current density $|J|$ at the transition from air to the conductor at the frequencies 5 and 165 GHz are shown. All curves are normalized to their maximum.

The S-parameter S_C of the connector interface ($p = 0$, left side) is simulated using CST Microwave Studio. A plug as shown in [5, Fig. 4] is fully described by measured values for the OCID, ICOD, pin diameter, and pin depth as well as values from technical drawings for male inner and male outer chamfers. Each parameter X_i is associated with a nominal value x_i and a standard uncertainty $u(x_i)$. During repeated simulations, each nominal value is varied by a small amount, typically 1 μ m, to calculate the sensitivities c_i . The value S_C is the simulation results based on the nominal values x_i , whereas the corresponding uncertainty $u(S_C)$ is given as [16]

$$u(S_C) = \sqrt{\sum_{i=1}^N (c_i \cdot u(x_i))^2}. \quad (1)$$

B. Effective Conductivity Modeling

The primary offset shorts are manufactured from copper–beryllium bulk material coated with a gold layer of approximately 1 μ m thickness. To accurately model losses in coaxial lines, work [17] extends the simple model of lossless conductors. To calculate the propagation constant in the lossy coaxial line and the reflection coefficient at the short plane, the frequency-dependent effective conductivity of the material is required. It can be calculated from surface roughness and dc conductivity using the model described in [18]. To take into account the gold coating, the improved layered model described in [19] is used.

The result for an exemplary multilayer conductor consisting of copper–beryllium coated with a 1- μ m gold layer in air is shown in Fig. 4. All curves are normalized to their respective maximum values. The dc conductivity (red solid) ranges from air ($\sigma_{dc} = 0$ MS/m) to gold ($\sigma_{dc} = 43$ MS/m with $h = 1$ μ m) to copper–beryllium ($\sigma_{dc} = 9$ MS/m). The surface roughness of both metals is assumed to be 150 nm and the susceptibility is set to zero for both materials. In addition to the dc conductivity profile, the magnetic field (blue dashed) and current density (orange dotted) distributions are shown at 5 and 165 GHz, respectively. At 5 GHz, the

TABLE II
OFFSET SHORT MATERIAL PARAMETERS AFTER OPTIMIZATION

offset short	C2	C3	C4	C5	C6	C7	C8
σ_c / MS/m	13.8	12.5	12.8	12.7	12.8	12.3	12.1
σ_b / MS/m	10	9.9	9.8	10.2	10	10.2	10
$R_{q,c}$ / nm	270	125	110	90	88	52	37
$R_{q,b}$ / nm	150	150	150	150	150	150	150
t_c / μ m	1.6	0.9	0.9	0.9	0.9	0.8	0.9

magnetic field penetrates the gold layer, and the current also flows within the copper–beryllium bulk material. The effective conductivity is therefore influenced by both materials and their respective material parameters. At 165 GHz, the magnetic field is confined to the 1- μ m gold layer, and the current flows predominantly within it, clearly illustrating the skin effect described in [15, p. 19]. Therefore, the effective conductivity is primarily determined by the outer gold layer.

For each of the seven primary offset short standards, the effective conductivity is calculated from the following.

- 1) DC conductivity of the outer, coating layer σ_c .
- 2) DC conductivity of the inner, bulk material σ_b .
- 3) Respective surface roughness $R_{q,c}$ and $R_{q,b}$.
- 4) Thickness of the outer, coating layer t_c .

As these values do not necessarily coincide with the nominal values of copper–beryllium and gold, the resulting values after optimization are summarized in Table II. Since the surface roughness $R_{q,b}$ of the bulk material has negligible influence on the result, the same value of 150 nm was assigned to all offset shorts, estimated from optical measurements performed with a laser scanning microscope. It is important to note that the same effective conductivity is used for both the outer and inner conductors, although they are manufactured in different ways, which in turn can only approximate the true parameter values.

C. S-Parameter Calculation

Using measured values for OCID and ICOD, the outer conductor length in conjunction with the pin depth, as well as the effective conductivity of the material, the line impedance and propagation constant are calculated according to [17] for each of the N segments with a length of 10 μ m. The two-port S-parameters $S_{L,i}$ with $i \in \{1, 2, \dots, N\}$ of the individual line segments are computed using a reference impedance of 50 Ω and are subsequently cascaded to form the complete line segment S_L of the offset short. The simulated connector S_C is cascaded on the left side and the short plane reflection coefficient s_S is calculated as described in [15] and cascaded on the right side

$$s_{11} = S_C \oplus (S_{L,1} \oplus \dots \oplus S_{L,N}) \oplus s_S. \quad (2)$$

The operation \oplus describes the cascading of two-port DUTs. Uncertainties are propagated using UncLib [7] by METAS together with MATLAB for all calculations and simulations. The influences of dimensional and material parameters are discussed in detail in [20].

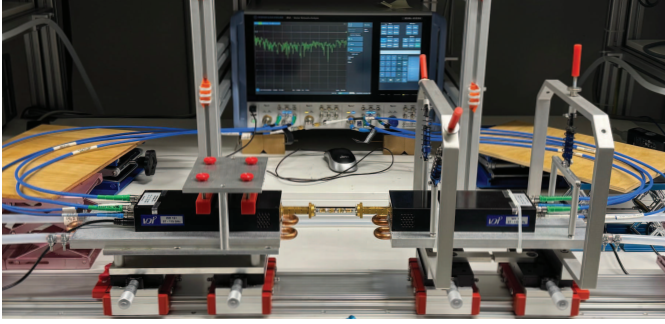


Fig. 5. Measurement setup using WR 10 frequency extensions. A *direct thru* measurement is used to copy error terms from one port to another according to [2]. Additionally, liquid cooling plates are mounted below the frequency extensions and a common LO signal is used for both ports.

III. S-PARAMETER MEASUREMENT SETUP

Measurements of primary calibration standards and several DUTs are carried out in three frequency ranges: below 67 GHz using a VNA without frequency extenders, up to 110 GHz using WR 10 frequency extenders, and up to 167 GHz using WR 7 frequency extenders. Only primary standards with plug connectors are used. Jack DUTs can be calibrated by transferring the error terms from one port (left side, e_1) to another (right side, e_2) using a direct thru connection (definition T and measurement M). This procedure, called copy calibration, is comparable to QSOLT calibration [21], explained in detail in [10] and described by

$$e_2 = (e_1 \oplus T)^{\oplus 1} \oplus M. \quad (3)$$

The operation $\oplus 1$ denotes matrix inversion of a two-port.

In comparison with previous work on PC 0.8 mm, the lower frequency limit for the overdetermined least-squares calibration is lowered to 10 GHz. This change is possible because of improved temperature stability and repeatability, and consequently better interpolation of the open and match standard used for the QSOLT calibration at frequencies below 10 GHz. The procedure as well as a special averaging scheme is described in detail in [2]. The measurements are performed in a laboratory with a controlled temperature of $23^\circ\text{C} \pm 1^\circ\text{C}$ and a relative humidity of 25%–35%.

The frequency extenders introduce additional heat at the waveguide interface and subsequently change the test port temperature: additional drift is introduced and can be especially observed in the reflection phase measurement results as well as degraded measurement repeatability. Furthermore, the S-parameters of the primary offset standards are calculated from dimensions at a temperature of 23°C . Therefore, water cooling plates are introduced to keep the waveguide temperature of the frequency extenders steady at $23^\circ\text{C} \pm 0.5^\circ\text{C}$ during the measurement. The measurement setup for the WR 10 band, in which the highest temperature rise is observed, is shown in Fig. 5.

The port, at which the primary calibration standards are measured, is located on the left side. The secondary port, which is calibrated using a direct thru connection as shown in Fig. 5, is mounted on the opposite, right side. It is suspended on springs to ensure optimal alignment between the two ports.

TABLE III
MEASUREMENT SEQUENCE FOR PC 0.8 MM

measurement group	port 1 - plug	port 2 - jack
1	thru & switch term	
2	one-port DUTs	-
3	thru & switch term	
4	-	one-port DUTs
5	thru & switch term	
6	two-port DUTs	
7	thru & switch term	

Additionally, a linear rail system is employed to enable precise positioning of the test ports. During measurement of the different frequency bands, different test-port adapters had to be used to go from PC 1.85 mm/WR 10/WR 7 to PC 0.8 mm. Nevertheless, as good agreement within the expanded uncertainty region is achieved in the overlapping frequency regions, the validity of the following results is not undermined.

The measurement sequence, including one-port as well as two-port DUTs, is summarized in Table III. Before and after each group of DUTs, a direct thru connection, including switch terms, is measured (groups 1, 3, 5, and 7). In group 2, one-port DUTs with a plug connector are measured, including the primary calibration standards as well as transfer calibration kits. These include open, short, match, and mismatch standards. In group 3, only a single measurement of the direct thru is conducted for copy calibration followed by group 4, in which one-port DUTs with a jack connector are measured. Followed by another direct thru measurement in group 5, group 6 includes newly measured two-port DUTs like a matched thru, a beatty line, and a semi-rigid cable assembly. As evident by this measurement sequence, cable movements cannot be avoided for two-port DUTs in this particular case. Especially, measurements, including VNA extenders, are highly sensitive regarding cable movements, although a phase correction can be applied [22]. As described in [23], “if more than one two-port DUT is to be measured, and cable movements must be avoided completely, one set of OSM standards has to be measured in between the DUT measurements to recalibrate one VNA port after the movement of one cable.”

A. Connection Repeatability

During the measurements, each DUT is connected multiple times to be able to thoroughly investigate the connector repeatability based on [10] and modified as presented in [2]. The resulting connector repeatabilities for all three measurement frequency bands are shown in Fig. 6. A significant improvement of up to 6 dB is achieved in the WR 10 band. Additionally, minor improvements of about 3 dB are achieved for measurements without frequency extenders up to 67 GHz and measurements in the WR 7 band. It is difficult to separate the actual, true connector repeatability from the superimposed short-term drift, caused by the fluctuating ambient temperature. The observed changes are attributed to the stabilization of the laboratory ambient and test port temperatures, which has reduced the superimposed short-term drift. In the past, the laboratory temperature fluctuated by

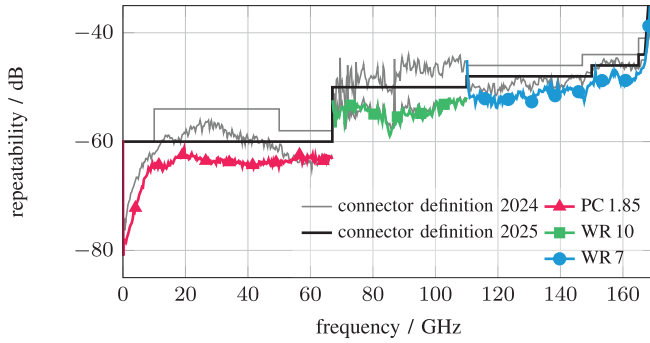


Fig. 6. Repeatability of PC 0.8 mm obtained during measurement in three frequency bands indicated by colored, marked lines. Gray lines are taken from [2]. Improvements are visible over the whole frequency range due to improved temperature stability of the laboratory and the measurement setup.

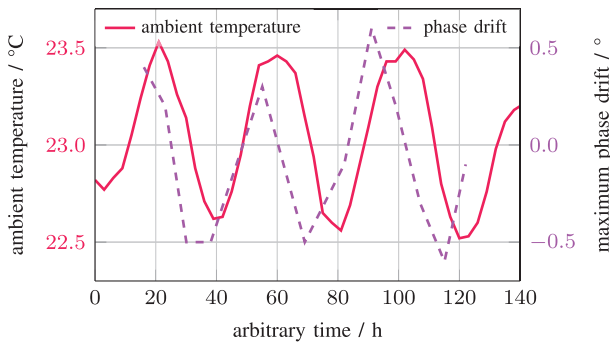


Fig. 7. Relation between ambient temperature fluctuations and maximum phase drift of different offset short standards at 67 GHz. A clear dependency between sinusoidal ambient temperature and phase drift is observed.

around 2 °C within 20 min, whereas now it only drifts by the aforementioned ± 1 °C within the entire measurement day. When discussing uncertainty budgets in Section IV, it is important to note that VNA drift does not include this short-term drift observed during repeatability assessment. It was characterized previously under stable ambient temperature conditions. Evaluating the different uncertainty contributions closely follows the procedure presented in [10] and [11].

To further assess the relationship between temperature fluctuations and phase drift, the ambient temperature is varied in a sinusoidal manner within 20 min between 22.5 °C and 23.5 °C as shown in Fig. 7. Several offset shorts are measured four times over a duration of approximately 6 min. For each standard, the maximum phase drift across the four measurements is determined at 67 GHz. When the ambient temperature is at its maximum or minimum, the phase drift is minimal, i.e., close to zero. In contrast, when the rate of temperature change is maximal, around 23 °C, the phase drift reaches its maximum. For this specific setup at 67 GHz, a temperature increase of 1 °C results in a phase drift of approximately 1°. This effect is mainly caused by additional short-term drift of the electronic measurement device rather than by thermal expansion of the standards.

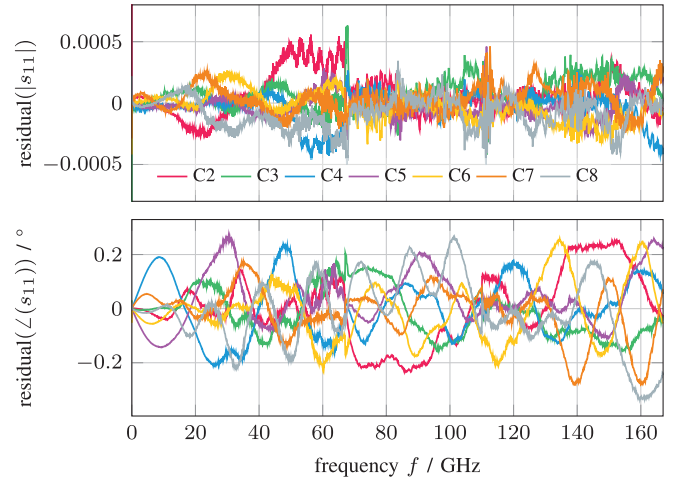


Fig. 8. Residuals of the overdetermined least-squares calibration using seven offset shorts C2–C8. Material parameters are optimized to minimize the differences (residuals) between the standard definition and the calibration result.

B. Calibration Standard Optimization

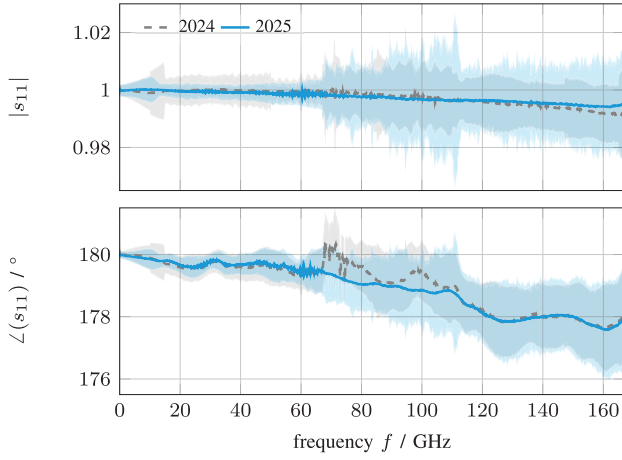
The metrics to be optimized in the overdetermined least-squares calibration are the calibration residuals, i.e., the differences between the calculated calibration standard definition and the measurement result obtained. Fig. 8 summarizes the result of the optimization: shown are residuals of magnitude and phase of the primary standards C2–C8. Offset short C2 exhibits the largest differences between 40 and 60 GHz. Insufficient characterization of the interface, artifacts during the measurement of the OCID, or eccentricity of the inner conductor are possible causes. Overall, good agreement is achieved, with maximum deviations of 0.0005 in magnitude and 0.25° in phase.

IV. MEASUREMENT AND CALIBRATION RESULTS

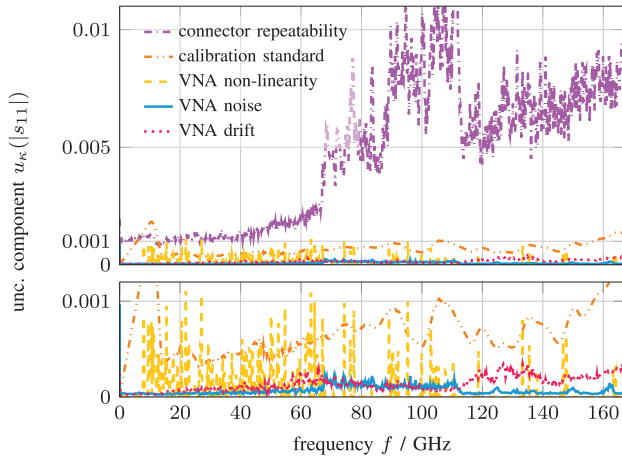
The error terms obtained from the overdetermined least-squares calibration in conjunction with the low-frequency results obtained through OSM calibration are used to de-embed further calibration standards and obtain error corrected measurement results traceable to the SI system. During primary calibration, a broadband OSM calibration kit specified up to 167 GHz is characterized, to allow fast calibration of customer DUTs in further experiments. Calibration results of the following DUTs are presented: high reflect DUTs (flush short and open), a low reflect DUT (broadband match), and a two-port DUT (beatty line).

A. Results of a Flush Short

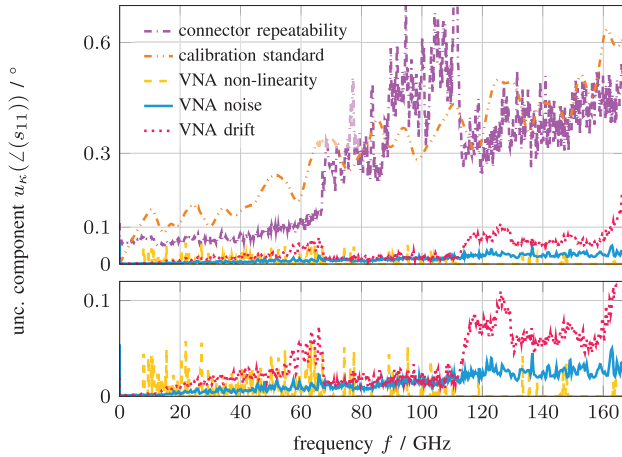
In addition to the seven primary offset short (C2–C8) standards used for optimization, a flush short (C1) with plug connector is measured for verification. The resulting reflection coefficient is shown in Fig. 9(a). The measurement closely matches the expected behavior of a flush short described in [10]: the magnitude is near unity and the phase remains close to 180°, but both decrease with increasing frequency.



(a)



(b)

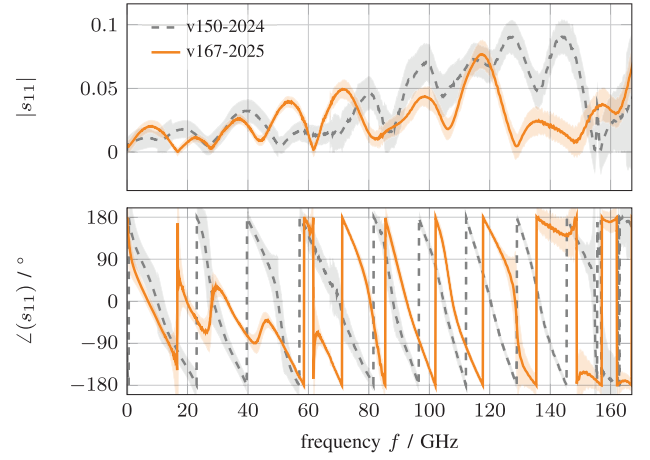


(c)

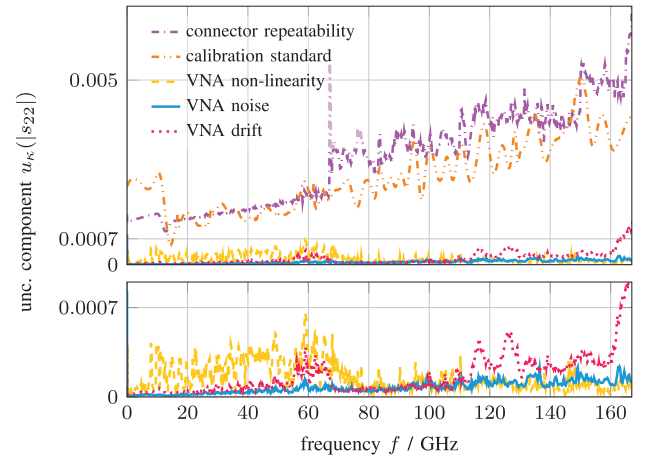
Fig. 9. (a) Reflection coefficient s_{11} of a flush short with plug connector obtained in 2024 [2] and 2025, including expanded uncertainties ($k = 2$). Good agreement is achieved between the two results. (b) As shown in the magnitude uncertainty budget, the connector repeatability represents the largest source of reflection magnitude uncertainty. Furthermore, the reflection phase uncertainty budget (c) indicates that the phase uncertainty is additionally influenced by the primary standard definitions.

This decline is consistent with the expected effects of limited effective conductivity of the short plane material.

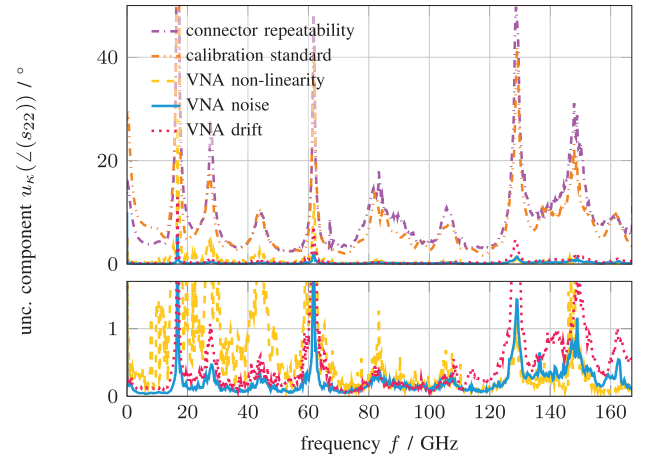
Additionally, values obtained during the 2024 primary experiment published in [2] are shown for comparison. The



(a)



(b)



(c)

Fig. 10. (a) Reflection coefficient s_{22} of a match specified up to 167 GHz with jack connector including expanded uncertainties ($k = 2$). Values of a match specified up to 150 GHz from [2] are shown additionally. (b) As shown in the magnitude uncertainty budget as well as (c) reflection phase uncertainty budget, the connector repeatability and the primary standard definitions represent the largest sources of uncertainty.

difference in magnitude is within the achieved expanded uncertainty interval, which decreased for the 2025 primary experiment due to improved repeatability of this specific DUT. Significant improvements are observed for the phase of the

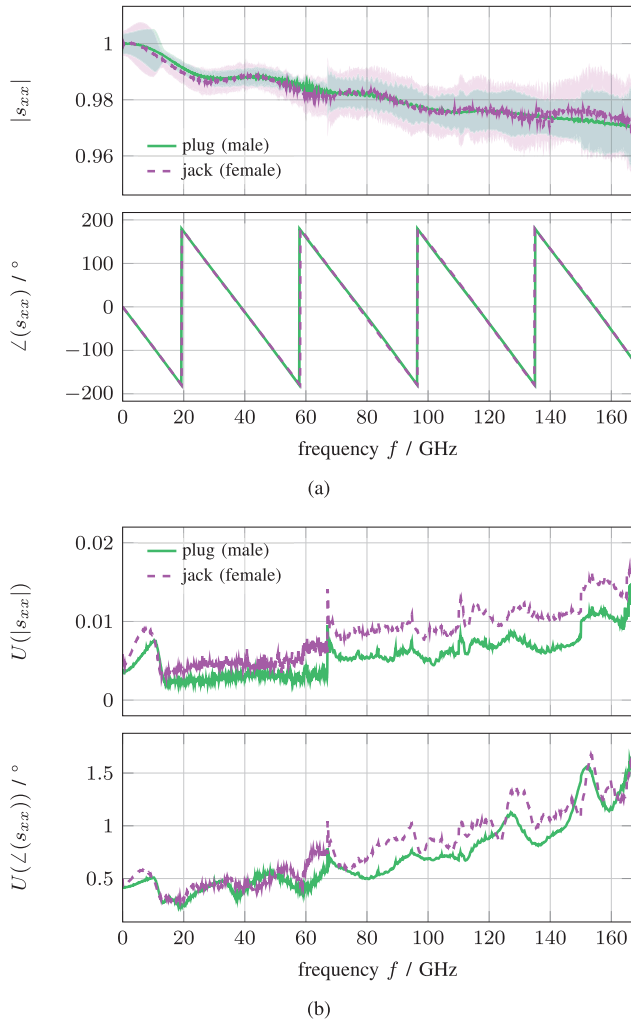


Fig. 11. (a) Reflection coefficients s_{xx} of two open terminations with plug (s_{11}) and jack (s_{22}) obtained during a primary experiment including expanded uncertainties ($k = 2$). For clarity, the expanded uncertainties ($k = 2$), shown again in (b), illustrate the effect on uncertainty of the copy calibration scheme.

flush short. In the 2024 primary experiment, temperature fluctuations caused problems in the WR 10 frequency range. These nonphysical discontinuities in phase are eliminated by providing a stable temperature in the laboratory and at the test port. Overall, good agreement between both experiments is observed, even though both experiments were carried out one year apart. Expanded uncertainties ($k = 2$) in reflection magnitude $U(|s_{11}|)$ of 0.002–0.03 and phase $U(\angle(s_{11}))$ of 0.1° – 1.95° are achieved.

To assess main uncertainty contributions, Fig. 9(b) and (c) shows the uncertainty budget of reflection magnitude and phase, respectively. Magnitude uncertainty is mainly influenced by the repeatability of the DUT. The second most influential contribution is the uncertainties associated with the primary standards. Phase uncertainty is highly dependent on the connection repeatability and the primary standard definition. Especially, the uncertainty of the outer conductor length measurement influences the phase uncertainty as it directly translates into the uncertainty of the position of the reference plane. As all primary standards are high reflect standards, the VNA receivers operate at approximately the same operating

point. Due to this correlation, the nonlinearity influence of the VNA is nearly negligible for the calibration.

B. Results of a Broadband Match

A broadband match specified up to 167 GHz is measured as part of the primary experiment. In contrast, the 2024 version was only specified up to 150 GHz and showed resonances around 152 and 156 GHz. Fig. 10(a) shows a comparison of the reflection coefficient. As expected, the 2025 version does not show resonances while still exhibiting very good performance of better than or equal to -20 dB (0.1 linear) in reflection magnitude over the whole frequency range. Expanded uncertainties ($k = 2$) in reflection magnitude $U(|s_{11}|)$ of 0.003–0.015 and phase $U(\angle(s_{11}))$ of 7° – 180° are achieved. Especially, phase uncertainty is highly dependent on the magnitude so that no direct comparison between the two measurement runs can be discussed here.

To assess main uncertainty contributions, Fig. 10(b) and (c) shows the uncertainty budget of reflection magnitude and phase, respectively. Magnitude and phase uncertainty are mainly influenced by connector repeatability as well as the primary standard definitions. Overall, phase uncertainty is inversely proportional to the actual magnitude value, i.e., smaller reflections directly translate to higher phase uncertainty. As the VNA receivers operate at different operating points when measuring low reflect DUTs, VNA nonlinearity is nonnegligible. The nonlinearity uncertainty contributions are not correlated anymore and therefore do not cancel each other out during de-embedding. Additionally, the influence of VNA nonlinearity increases for smaller reflection coefficients.

C. Results of a Broadband Open

Additionally, two open terminations with plug (male) and jack (female) connectors are presented. Fig. 11(a) shows the resulting reflection coefficients. Both DUTs have similar electrical lengths, which can be seen in the near identical phase. The magnitude of both connector types coincides within their attributed expanded uncertainty, which is remarkable considering the asymmetric calibration scheme described in Section III. This underlines the validity of transferring error terms from one port to another using a direct thru connection.

For better comparison of uncertainties and to assess the influence of the copy calibration, Fig. 11(b) shows the uncertainties of (a). The influence of the direct thru can be seen clearly; the increased uncertainty of the magnitude in particular results primarily from the additional repeatability contribution. Spikes, observable around 67 and 110 GHz, can be traced back to the fact that these frequencies are near the upper operating limit of the VNA and WR 10 frequency extender, respectively.

D. Results of a Beatty Line

In addition to the one-port DUTs presented above, a beatty line is measured as a two-port device. It is part of a commercially available calibration kit specified up to 145 GHz and can be used for verification of the calibration process [10].

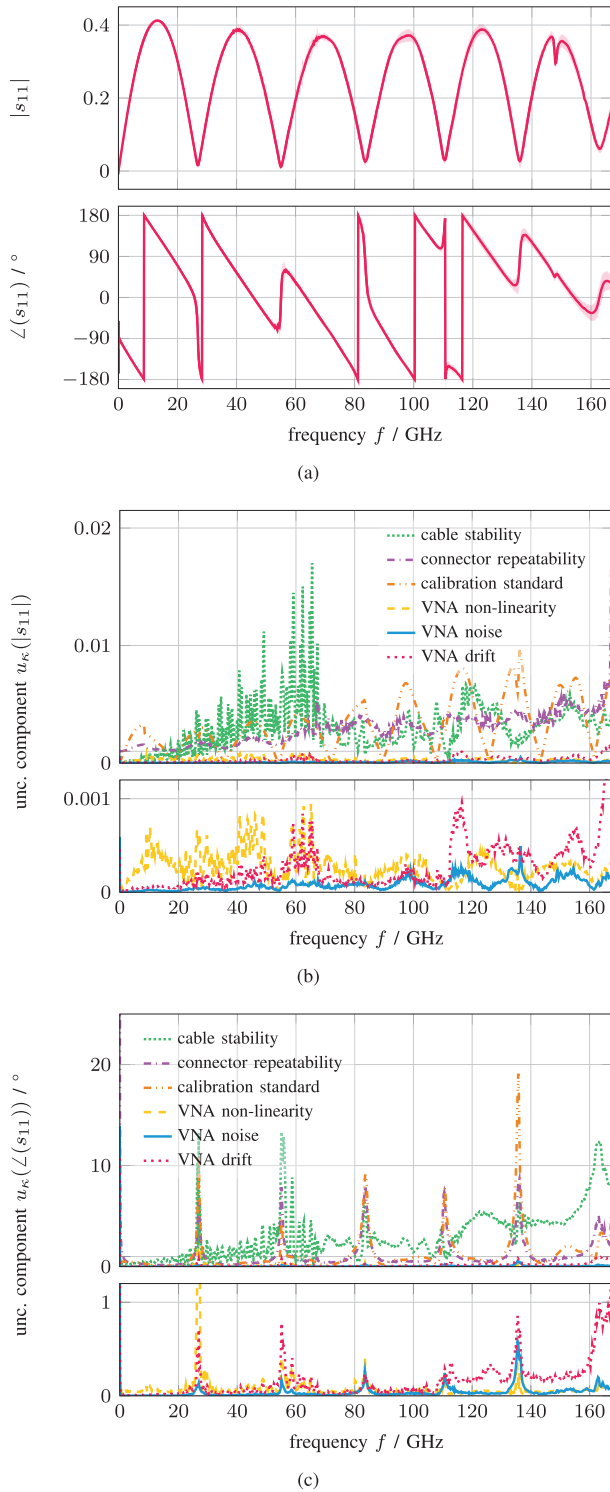


Fig. 12. (a) Reflection coefficient s_{11} of a beatty line specified up to 145 GHz, including expanded uncertainties ($k = 2$). As shown in the magnitude uncertainty budget (b) as well as the reflection phase uncertainty budget (c), the connector repeatability, primary standard definitions, and newly added cable stability represent the largest sources of uncertainty. Cable movement can be avoided as described in [23].

Fig. 12 summarizes the results of the reflection coefficient s_{11} at port 1. This port was moved during calibration so that an additional uncertainty contribution for cable stability is added during uncertainty evaluation. The reflection magnitude in Fig. 12(a) shows the expected behavior of a beatty line; at

even multiples of the fundamental frequency $f_0 = 13.5$ GHz, the reflection magnitude is minimal ($|s_{11}| \leq 0.06$). At odd multiples of f_0 , the reflection magnitude reaches its maximum of $|s_{11}| \approx 0.39$. Datasheet values for the line length and the impedance step are not available. The step length is estimated to be approximately 5.5 mm, and the impedance value is estimated to be around 32–35 Ω (inner conductor diameter around 0.46 mm). Expanded uncertainties ($k = 2$) in reflection magnitude $U(|s_{11}|)$ of 0.005–0.022 are achieved and phase $U(\angle(s_{11}))$ of 3°–43° are achieved. Although these uncertainties are higher than those of, for example, the match in Section IV-B, this is attributed to decreased repeatability during this particular measurement, which will be improved upon in future measurements. Since cable movement has no significant impact on the reflection [22], it can be expected that uncertainties in the range of the match are easily achievable. At around 148 GHz, a resonance can be observed, which is most likely caused by the bead and fits the specification of the calibration kit up to 145 GHz.

Looking at the magnitude uncertainty budget in Fig. 12(b), the main uncertainty contributions are the connector repeatability and primary calibration standard definitions. Additionally, cable stability is a significant contributor of uncertainty. The uncertainty budget for phase in Fig. 12(c) reveals the same conclusion as in Fig. 10(b). Small magnitude values at even multiples of f_0 result in high phase uncertainty.

Fig. 13 summarizes the results of the transmission coefficient s_{12} after correction of the phase according to [22]. As port 1 was moved during measurement and no new OSM standards are measured, as proposed in [23] to reduce uncertainty, cable stability is expected to be a dominant factor for transmission coefficient. The transmission magnitude and phase are shown in Fig. 13(a). Analogous to the reflection magnitude, the transmission magnitude shows the expected behavior of a beatty line: at even multiples of f_0 the magnitude reaches its maximum value, whereas for uneven multiples of f_0 , the magnitude reaches its minimal value. The phase is continuous and increases linearly with frequency. Expanded uncertainties ($k = 2$) in reflection magnitude $U(|s_{12}|) \leq 0.1$ dB are achieved and the phase $U(\angle(s_{12}))$ of 0.1°–5° is achieved. Factoring out cable stability, expanded uncertainties ($k = 2$) in reflection magnitude $U(|s_{12}|) \leq 0.007$ dB and phase $U(\angle(s_{12})) \leq 0.7^\circ$ are achievable. At around 148 GHz, a resonance can be observed, which is most likely caused by the bead and fits the specification of the calibration kit up to 145 GHz as well previous observations on reflection magnitude.

Looking at the magnitude uncertainty budget in Fig. 13(b) and the phase uncertainty budget in Fig. 13(c), the defining uncertainty contribution is cable stability as predicted in [22]. When factoring out the cable stability, e.g., by measuring an OSM calibration kit after the two-port DUT [23], the remaining uncertainties are mainly influenced by the connector repeatability and the primary calibration standard definitions. For phase uncertainty, VNA drift also plays a role, because the measurement sequence shown in Table III indicates the long timespan between the measurement of the primary calibration standards and the beatty line.

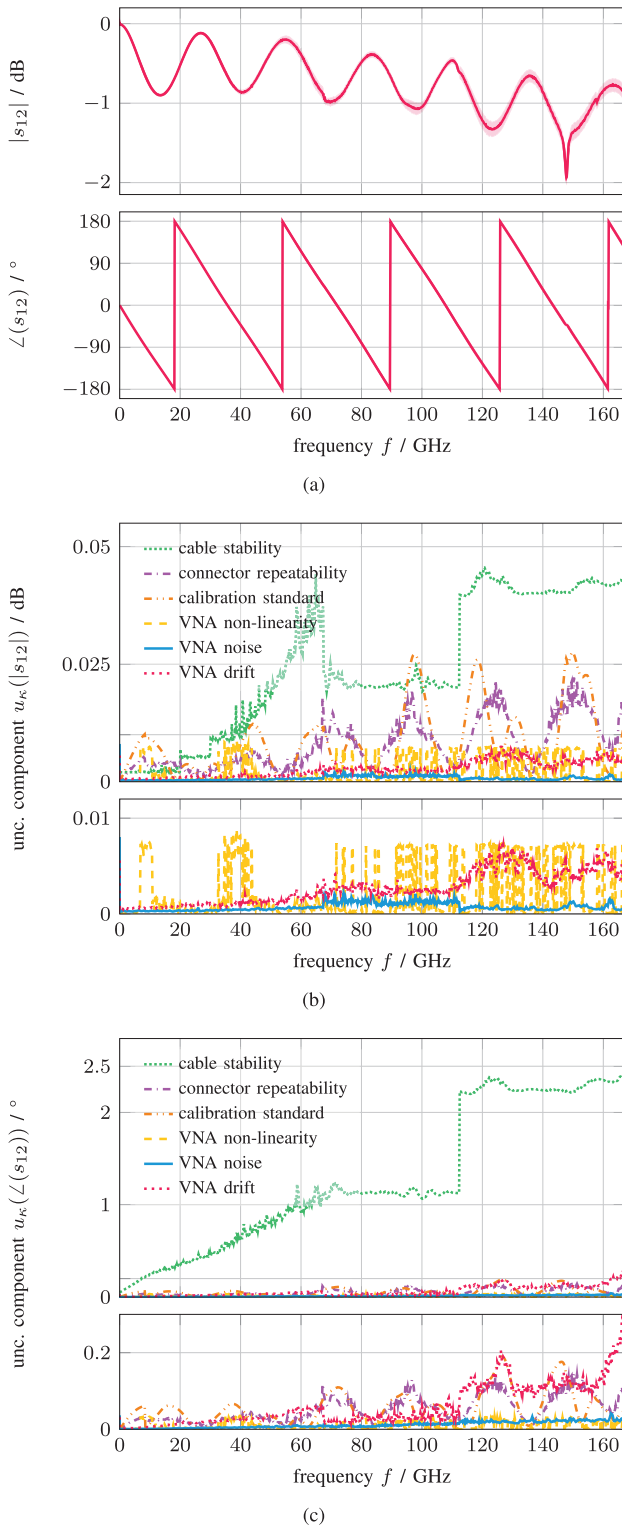


Fig. 13. (a) Transmission coefficient s_{12} of a beatty line specified up to 145 GHz, including expanded uncertainties ($k = 2$). Phase angle correction according to [22] is performed. As shown in the magnitude uncertainty budget (b) as well as the reflection phase uncertainty budget (c), the newly added cable stability represents the dominating sources of uncertainty. Cable movement can be avoided as described in [23], leaving connector repeatability, primary standard definitions, and VNA drift as the main uncertainty sources.

V. CONCLUSION

This article summarizes recent advancements in traceable metrology for the 0.8 mm PC. Significant improvements,

including enhanced overall repeatability of around 3–6 dB, are achieved. Furthermore, the maximum frequency, at which traceable measurements are feasible, has been extended from 165 to 167 GHz, enabling calibration across 98.4% of the maximum bandwidth of PC 0.8 mm. The required primary standards are dimensionally characterized and subsequently analyzed using analytic models and simulations. Using an overdetermined least-squares calibration involving seven offset short standards, traceability of one-port and two-port DUTs to the SI is established. Calibration results, including uncertainty budgets for magnitude and phase, are presented and discussed for different DUTs.

The main uncertainty contributions for one-port DUTs are the connection repeatability and the standard definition of the primary offset short standards. Especially, the uncertainty of the length measurement is highly influential on reflection magnitude and phase uncertainty. To improve the repeatability, the temperature of the laboratory is stabilized to $23^\circ\text{C} \pm 1^\circ\text{C}$. For two-port DUTs, cable stability is the critical uncertainty contribution. To achieve small uncertainties, the movement of cables can be avoided by measuring additional OSM standards after the two-port DUT [23].

Overall, these improvements reinforce the metrological robustness of the 0.8 mm PC: small uncertainties, good connection repeatability, as well as mechanical stability. Calibration and measurement capabilities (CMCs), which describe the calibration portfolio of a national metrology institute, for various physical measurements are compiled in the Key Comparison Database (KCDB) [24], maintained by the Bureau International des Poids et Mesures (BIPM). Regarding PC 0.8 mm, CMCs are submitted for reflection measurements and will be extended to transmission measurements in the near future. To further enhance measurement quality and confidence, a common additional test port adapter from PC 0.8 mm to PC 0.8 mm will be used in the future, to provide the same test-port interface independent of the measurement setup. During the measurements shown in Section IV, no such adapter specified up to 167 GHz was yet commercially available. A comparison between time and frequency domain measurements comparable to [25] is currently being conducted using an electrooptic sampling setup and will be published in the future.

ACKNOWLEDGMENT

The authors thank Rohde&Schwarz GmbH and Company KG and SPINNER GmbH for valuable and productive discussions. SPINNER GmbH is to be thanked additionally for fabricating the necessary primary offset standards, DUTs, and adapters. They disclose the usage of ChatGPT version 5 [26] for spellchecking and grammar enhancement.

REFERENCES

- [1] W. K. Perangin-Angin, K. Kuhlmann, and J. Rühaak, "Dielectric waveguide as transmission line for R 1.8k microcalorimeter," in *Proc. Conf. Precis. Electromagn. Meas. (CPEM)*, Denver, CO, USA, Jul. 2024, pp. 1–2, doi: [10.1109/CPEM61406.2024.10646069](https://doi.org/10.1109/CPEM61406.2024.10646069).
- [2] A. Schramm, F. Gellersen, F. Rausche, and K. Kuhlmann, "Traceable S-parameter measurements up to 165 GHz using 0.8 mm coaxial standards," *IEEE Microw. Wireless Technol. Lett.*, vol. 35, no. 6, pp. 936–939, Jun. 2025, doi: [10.1109/LMWT.2025.3562419](https://doi.org/10.1109/LMWT.2025.3562419).

- [3] IEEE Standard for Precision Coaxial Connectors at RF, Microw., and Millimeter-Wave Frequencies—Part 1: General Requirements, Definitions, and Detailed Specifications, Standard 287.1-2021, Sep. 2022, doi: [10.1109/IEEESTD.2022.9889249](https://doi.org/10.1109/IEEESTD.2022.9889249).
- [4] D. Stokes, F. Gellersen, D. Allal, J. Skinner, G. N. Phung, and K. Kuhlmann, "Traceable S-parameter measurements up to 90 GHz in 1.35 mm coaxial," *Meas. Sci. Technol.*, vol. 34, no. 6, Mar. 2023, Art. no. 064006, doi: [10.1088/1361-6501/acc04c](https://doi.org/10.1088/1361-6501/acc04c).
- [5] J. Hoffmann, M. Wollensack, J. Ruefenacht, D. Stalder, and M. Zeier, "Traceable calibration with 1.0 mm coaxial standards," in *Proc. 87th ARFTG Microw. Meas. Conf. (ARFTG)*, San Francisco, CA, USA, May 2016, pp. 1–4, doi: [10.1109/ARFTG.2016.7501943](https://doi.org/10.1109/ARFTG.2016.7501943).
- [6] D. Blackham, "Application of weighted least squares to OSL vector error correction," in *Proc. 61st ARFTG Conf. Dig.*, Philadelphia, PA, USA, Jun. 2003, pp. 11–21, doi: [10.1109/ARFTGS.2003.1216862](https://doi.org/10.1109/ARFTGS.2003.1216862).
- [7] M. Zeier, J. Hoffmann, and M. Wollensack, "Metas.UncLib—A measurement uncertainty calculator for advanced problems," *Metrologia*, vol. 49, no. 6, pp. 809–815, Nov. 2012, doi: [10.1088/0026-1394/49/6/809](https://doi.org/10.1088/0026-1394/49/6/809).
- [8] The MathWorks Inc., Natick, MA, USA. (2023). *MATLAB Version: 9.14.0 (R2023a)*. [Online]. Available: <https://www.mathworks.com>
- [9] Dassault Systèmes. (2023). *CST Microwave Studio 2023*. [Online]. Available: <https://www.3ds.com/products/simulia/cst-studio-suite>
- [10] M. Zeier, D. Allal, and R. Judaschke, "Guidelines on the evaluation of vector network analysers (VNA)—Euramet calibration guide, no. 12 (CG-12)," Euramet e.v., Braunschweig, Germany, Tech. Rep. Version 3.0, Mar. 2018.
- [11] M. Wollensack, J. Hoffmann, J. Ruefenacht, and M. Zeier, "VNA tools II: S-parameter uncertainty calculation," in *Proc. 79th ARFTG Microw. Meas. Conf.*, Jun. 2012, pp. 1–5, doi: [10.1109/ARFTG79.2012.6291183](https://doi.org/10.1109/ARFTG79.2012.6291183).
- [12] W. Wiatr and A. Lewandowski, "Multiple reflect technique for wideband one-port VNA calibration," in *Proc. Int. Conf. Microw., Radar Wireless Commun.*, Krakow, Poland, May 2006, pp. 37–40, doi: [10.1109/MIKON.2006.4345100](https://doi.org/10.1109/MIKON.2006.4345100).
- [13] W. Wiatr, "Line-length optimization of offset-short standards for broadband VNA calibration," in *Proc. 18-th Int. Conf. Microw., Radar Wireless Commun.*, Vilnius, Lithuania, Jun. 2010, pp. 1–4.
- [14] J. P. Dunsmore, *Handbook of Microwave Component Measurements: With Advanced VNA Techniques*, 2nd ed., Hoboken, NJ, USA: Wiley, 2020.
- [15] D. M. Pozar, *Microwave Engineering*, 4th ed., Hoboken, NJ, USA: Wiley, 2012.
- [16] *Evaluation of Measurement Data—Guide to the Expression of Uncertainty in Measurement*, document JCGM 100:2008, BIPM, IEC, IFCC, ILAC, ISO, IUPAC, IUPAP, and OIML, Joint Committee for Guides in Metrology, Sep. 2008.
- [17] W. C. Daywitt, "First-order symmetric modes for a slightly lossy coaxial transmission line," *IEEE Trans. Microw. Theory Techn.*, vol. 38, no. 11, pp. 1644–1650, Nov. 1990, doi: [10.1109/22.60011](https://doi.org/10.1109/22.60011).
- [18] G. Gold and K. Helmreich, "A physical model for skin effect in rough surfaces," in *Proc. 7th Eur. Microw. Integr. Circuit Conf.*, Amsterdam, The Netherlands, Oct. 2012, pp. 631–634.
- [19] G. Gold and K. Helmreich, "Modeling of transmission lines with multiple coated conductors," in *Proc. 46th Eur. Microw. Conf. (EuMC)*, Oct. 2016, pp. 635–638, doi: [10.1109/EuMC.2016.7824423](https://doi.org/10.1109/EuMC.2016.7824423).
- [20] A. Schramm, F. Gellersen, and K. Kuhlmann, "Influence of dimensional and material parameters and their uncertainties on calculable offset shorts," in *Proc. 53rd Eur. Microw. Conf. (EuMC)*, Berlin, Germany, Sep. 2023, pp. 620–623, doi: [10.23919/EUMC58039.2023.10290258](https://doi.org/10.23919/EUMC58039.2023.10290258).
- [21] A. Ferrero and U. Pisani, "QSOLT: A new fast calibration algorithm for two port s parameter measurements," in *Proc. 38th ARFTG Conf. Dig.*, San Diego, CA, USA, Dec. 1991, pp. 15–24, doi: [10.1109/ARFTG.1991.324034](https://doi.org/10.1109/ARFTG.1991.324034).
- [22] F. K. H. Gellersen, D. Ulm, F. Rausche, A. T. Schramm, and K. Kuhlmann, "Influence of LO cable movements on VNA measurements using frequency extensions," *Adv. Radio Sci.*, vol. 22, pp. 47–52, Nov. 2024, doi: [10.5194/ars-22-47-2024](https://doi.org/10.5194/ars-22-47-2024). [Online]. Available: <https://ars.copernicus.org/articles/22/47/2024/>
- [23] K. Kuhlmann, F. Gellersen, and M. Tschauder, "Comparison of S-parameter measurement methods for adapters," *Adv. Radio Sci.*, vol. 20, pp. 1–8, Mar. 2023, doi: [10.5194/ars-20-1-2023](https://doi.org/10.5194/ars-20-1-2023). [Online]. Available: <https://ars.copernicus.org/articles/20/1/2023/>
- [24] Bureau International des Poids et Mesures (BIPM). *Key Comparison Database (KCDB)*. Accessed: Jun. 27, 2025. [Online]. Available: <https://www.bipm.org/kcdb/>
- [25] M. Bieler and U. Arz, "Characterization of high-frequency interconnects: Comparison between time- and frequency-domain methods," in *Proc. IEEE 20th Workshop Signal Power Integrity (SPI)*, Turin, Italy, May 2016, pp. 1–4, doi: [10.1109/SAPIW.2016.7496271](https://doi.org/10.1109/SAPIW.2016.7496271).
- [26] OpenAI, Inc., San Francisco, CA, USA. (2025). *ChatGPT (GPT-5)*. [Online]. Available: <https://chat.openai.com>



Andreas Tobias Schramm (Member, IEEE) received the master's (M.Sc.) degree from the Technical University of Brunswick, Brunswick, Germany, in 2022, where he is currently pursuing the Dr.-Ing. degree.

He has been at the Physikalisch-Technische Bundesanstalt, Brunswick, since 2014. His current research interests include metrology at millimeter-wave frequencies, especially for impedance and S-parameter measurements.



Frauke Kathinka Helene Gellersen received the Dr.-Ing. degree from the Technical University Hamburg-Harburg, Hamburg, Germany, in 2018.

She has been at the Physikalisch-Technische Bundesanstalt, Brunswick, Germany, since 2019. Her current research interests include metrology at millimeter-wave frequencies, especially for high-frequency voltage, impedance, and S-parameter measurements.

Florian Rausche received the Dipl.-Ing. degree from FH Wolfenbüttel, Wolfenbüttel, Germany, in 2008.

He has been at the Physikalisch-Technische Bundesanstalt, Brunswick, Germany, since 2009. His current research interests include S-parameter measurements for coaxial and waveguide transmission lines.



Karsten Kuhlmann received the Dipl.-Ing. degree from the Technical University Brunswick, Brunswick, Germany, in 2004, and the Dr.-Ing. degree from the Technical University Hamburg-Harburg, Hamburg, Germany, in 2009.

He has been at the Physikalisch-Technische Bundesanstalt, Brunswick, Germany, since 2009. His current research interests are the realization and dissemination of the RF base quantities: voltage, power, attenuation, and scattering parameters.